Distributed Real-Time Optimal Power Flow Control in Smart Grid

Yun Liu, *Member, IEEE*, Zhihua Qu, *Fellow, IEEE*, Huanhai Xin, *Member, IEEE*, and Deqiang Gan, *Senior Member, IEEE*

***Abstract*—Conventionally, power system has a hierarchical control structure including primary, secondary, and tertiary controls. The drawbacks of this hierarchical scheme are manifest: 1) it lacks flexibility and scalability, which is against the trend toward an open-access power system; 2) load forecast as the basis of tertiary control could be inaccurate and infeasible, especially in microgrid for example; 3) as the penetration of renewable energy increases, the relatively long time-scales of secondary and tertiary controls cannot accommodate to more severe power fluctuation within the system. To avoid these drawbacks, a distributed real-time optimal power flow control strategy is introduced in this paper. With the aid of up-to-date smart grid technologies such as two-way communication and distributed sensor, the proposed approach can avoid the need of load forecast and achieve the same objective as hierarchical control with a feedback mechanism in real time, that is to recover the nominal system frequency and maintain the active power of the generators close to the optimal operational condition in the presence of any disturbance. Convergence of the proposed approach is analytically proved. Simulation results in a 34-bus islanded microgrid and the IEEE 118-bus bulk power grid validate the effectiveness and efficiency of the proposed approach.**

***Index Terms*—Consensus, distributed control, frequency regulation, multi-agent system, optimal power flow.**

I. Introduction

POWER systems have conventionally been operated in a hierarchical structure with the control layers separated in different time-scales [1]–[3]. The primary control stabilizes system frequency in the transient after disturbance: it adjusts the power output of generators in response to frequency deviation according to the power/frequency droop curve, which leads to a steady-state frequency deviation. In a longer time-scale, the secondary frequency control restores system frequency to its nominal value with automatic generation control (AGC). In the longest time-scale, the tertiary control facilitates economic dispatch by setting the nominal power output of each generator to the optimal power flow (OPF) solution, which minimizes the total generation cost under a set of constraints (e.g., power balance, generation limit, and power flow limit constraints, etc.) based on load and generation forecast [4].

However, although the hierarchical control will remain active for the next decades, its shortcomings are quite manifest:

1) The large-scale integration of renewable energy increases the power fluctuation within power systems. Due to relatively slow reaction of the secondary control, frequency deviation caused by the primary control can be more severe, which may limit system stability or even trigger emergency control. The tertiary control is executed in the period of a quarter hour to half an hour. During each period, this power fluctuation can make the actual operational condition deviate from the optimal one, resulting in less economy efficiency.
2) The tertiary control based on OPF solution is not completely accurate due to the unavoidable load forecast error. In particular, accurate load forecast in a micro-grid is even more difficult, and could be costly [5].
3) As the diversity and quantity of energy resources increase, open access is a trend for both micro-grids [3] and bulk power grids [6], [7]. The conventional top-down hierarchical scheme, which is suitable for the coordination of centralized generation, is inconsistent with this trend due to its lack of flexibility and scalability, as well as the need of expensive high-performance computing system and high-bandwidth communication system.

The concept of smart grid, which refers to a modernized grid controlled by computer-based automation and two-way communication structures, provides a new tool in power system design, control and optimization [8], [9]. With the aid of these up-to-date smart grid technologies, distributed algorithms based on the multi-agent system (MAS) have been extensively applied to power systems in the past decade: in [10], the authors initiatively apply a consensus algorithm to solve economic

Manuscript received January 5, 2016; revised May 17, 2016, July 31, 2016, and October 18, 2016; accepted November 29, 2016. Date of publication December 5, 2016; date of current version August 17, 2017. The work of Y. Liu, H. Xin, and D. Gan was supported by the National High Technology Research and Development Program of China (No. 2015AA050202), the National Natural Science Foundation of China (No. 51577168), and the State Grid Zhejiang Electric Power Company (Study on Planning Mode of Active Distribution Network in Zhejiang Province, No. 5211JY15001Q). The work of Z. Qu was supported in part by U.S. National Science Foundation under Grant ECCS-1308928, in part by U.S. Department of Energy awards DE-EE0006340 and DE-EE0007327, in part by U.S. Department of Transportation Grant DTRT13-G-UTC51, in part by L-3 Communication contract 11013I2034, in part by Leidos contract P010161530, and in part by Texas Instruments awards. Paper no. TPWRS-00026-2016.

Y. Liu was with the University of Central Florida, Orlando, FL 32816 USA. He is now with the Energy Research Institute, Nanyang Technological University, Singapore 639798, and also with the Department of Electrical Engineering, Zhejiang University, Hangzhou 310027, China (e-mail: yunliu@ntu.edu.sg).

Z. Qu is with the Department of Electrical and Computer Engineering, University of Central Florida, Orlando, FL 32815 USA (e-mail: qu@ucf.edu).

H. Xin was with the University of Central Florida, Orlando, FL 32816 USA. He is now with the Department of Electrical Engineering, Zhejiang University, Hangzhou 310027, China (e-mail: xinhh@zju.edu.cn).

D. Gan is with the Department of Electrical Engineering, Zhejiang University, Hangzhou 310027, China (e-mail: deqiang.gan@ieee.org).

Color versions of one or more of the figures in this paper are available online at http://ieeexplore.ieee.org.

Digital Object Identifier 10.1109/TPWRS.2016.2635683

dispatch problem by driving the incremental cost of each generator to a common value, but this method requires global information (aggregated generation output) to be collected by a leader generator, which is practically difficult to be acquired in real time. Reference [11] solves the same problem by distributively and collectively estimating the mismatch between demand and aggregated power output of the generators, which is used as a feedback mechanism to adjust the power output of each generator. Different from the above literature, reference [12] proposes an online optimal generation control method, which can recover the nominal system frequency and minimize the total generation cost simultaneously. Reference [13] achieves the hierarchical control in micro-grid in a fully decentralized way, which does not require any communication among the distributed generators (DGs). Reference [14] achieves economic operation and secondary frequency regulation simultaneously through local feedback control. However, all of the aforementioned work has a common limitation: they only consider power balance and generation limit constraints. In practice, power flows can never exceed their thermal limits, otherwise, it will result in overheating of the power lines and contingencies may happen to the grid. This problem becomes more prominent recently since today's power grid is operated closer to its capacity limit [15]. Therefore, power flow limit constraints must be considered in power system dispatch/control [4], [16].

Based on the distributed cooperative control theory [17], a distributed real-time optimal power flow (RTOPF) control approach, which integrates the function of hierarchical control, is introduced in this paper. This approach is applicable to coordination of active power of synchronous generators and virtual power plants [18], [19] in bulk power grids, or to that of DGs (e.g., photovoltaic systems, wind generators, micro turbines, fuel cells, etc.) in islanded MV/HV micro-grids [20]. A full consideration on all the cases of a micro-grid operating in the grid-tied mode is out of the scope of this work. It is worth noting that DGs in the rest of this paper are considered to be dispatchable with control methods provided in [21]–[23] (while the undispatchable DGs are viewed as negative loads). For simplicity, the different forms of energy resources in both islanded micro-grids and bulk power grids are collectively called generation units (GUs). Different from the hierarchical scheme, where economic dispatch is fulfilled with feed-forward control based on load forecast, the proposed control runs in real time in a close-loop fashion to dynamically adjust the power generation set-points of the primary frequency control of GUs by means of communication among geographically neighboring GUs and distributed sensors measuring power flows. As a result, the function of the hierarchical control is simultaneously achieved, i.e., the frequency deviation converges to zero in the steady state, while the generation cost is minimized under power balance, power flow limit, and generation limit constraints.

The proposed approach has several distinct features:

1) Thermal limit constraint is handled by distributively measuring power flows, which avoids the estimation of global information, leads to a faster convergence, and is also in line with the trend of smart grid.

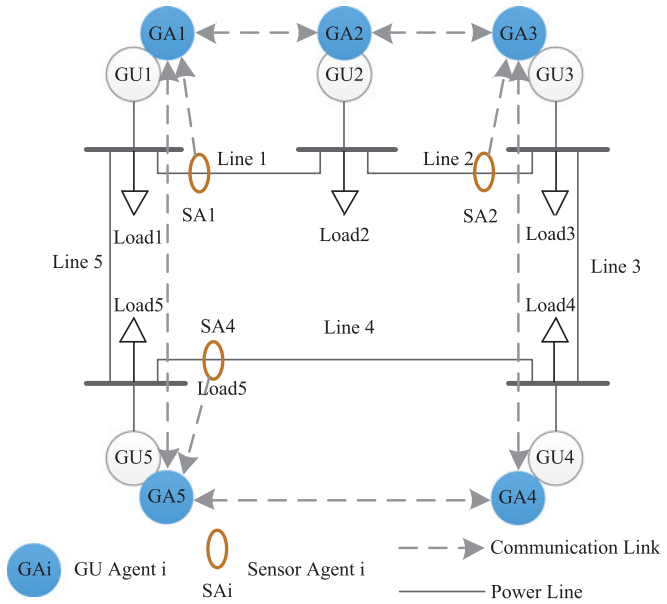

Fig. 1. Illustration of the proposed control scheme.

2) It is an upper-level control, which only adjusts power generation set-points of the speed governors and thus is compatible with various forms of GU controllers.
3) It can accommodate to time-varying generation limits, which is important especially for DGs since their maximum available power depends on the weather condition.
4) A connected two-way communication network that facilitates information exchanges among the GUs is a sufficient condition for convergence to a small neighborhood around the global optimum.
5) It is robust to communication interruptions and packet drops, and is plug-and-play for all sorts of GUs.

The rest of the paper is organized as follows. Section II formulates the problem of RTOPF control. Section III introduces the distributed RTOPF control approach. Simulation results and conclusions are presented in Section IV and V, respectively.

II. Problem Formulation

An MAS is a computerized system composed of multiple interacting intelligent agents within certain environment. It has been widely adopted as a feasible solution for managing complex distributed systems [17], [24]. This is motivated by its inherent benefits such as flexibility, scalability, autonomy and reduction in problem complexity among other factors [25]. In this paper, a smart grid is modeled and controlled as an MAS, where each agent can represent either a GU agent or a distributed sensor agent. GU agents control the power output of GUs, and are interconnected with a two-way communication network. The distributed sensor agents measure power flows of critical power lines in real time and interact with the GU agents, as illustrated in Fig. 1, where power flows of Lines 1, 2 and 4 are monitored for example.

In a power grid, a GU can be equivalently modeled with the classic swing equations [1], [26]

$$\dot{\theta}_i = \omega_i - \omega_0, \qquad \forall i \in \mathcal{S}_{\rm gen} \tag{1}$$

$$T_i\dot{\omega}_i = P_{G,i} - P_{e,i}, \ \ \forall i \in \mathcal{S}_{\rm gen} \tag{2}$$

where $\mathcal{S}_{\rm gen} = \{1, \cdots, q\}$ is the set of GUs; θ_i is the phase angle at the ith bus; T_i is the time constant representing the rotor inertia of ith GU (p.u.); $P_{G,i}$ and $P_{e,i}$ are power generated from the ith GU and power injection to the ith bus, respectively; $\omega_0 = 1$ p.u. and ω_i are the nominal frequency and frequency at the ith bus, respectively.

The governor provides primary frequency control to each GU. The power output $P_{G,i}$ is determined by the power/frequency droop curve described as

$$P_{G,i} = P_i^0 - k_{Di}\Delta\omega_i, \tag{3}$$

where P_i^0 is the power generation set-point of the ith GU, $\Delta\omega_i = \omega_i - \omega_0$ is the frequency deviation measured at the ith bus, and k_{Di} is a predefined frequency droop coefficient.

Without loss of generality, consider that $\mathcal{S}_{\rm load} = \{q+1, \cdots, n\}$ denotes the set of load buses, and each load adopts the constant power model.

Physically, GUs and loads are coupled by the non-linear AC power flow. Due to the coupling of active and reactive power flows, AC power flow is generally solved iteratively, which is computationally burdensome for real-time control. In this paper, we only study active power control by disassociating it from reactive power control for simplicity. As for reactive power dispatch, distributed control and optimization methods have been investigated in details, for example, in [27], [28].

The active/reactive power injection through the ith bus can be written as

$$P_{e,i} = \sum_{(i,j)\in\mathcal{S}_{\rm line}} E_iE_j\big[g_{ij}\cos(\theta_i-\theta_j) + b_{ij}\sin(\theta_i-\theta_j)\big], \tag{4}$$

$$Q_{e,i} = \sum_{(i,j)\in\mathcal{S}_{\rm line}} E_iE_j\big[g_{ij}\sin(\theta_i-\theta_j) - b_{ij}\cos(\theta_i-\theta_j)\big], \tag{5}$$

while the active power flow through line $(i,j) \in \mathcal{S}_{\rm line}$ can be written as

$$F_{i,j} = g_{ij}E_i\big[E_i - E_j\cos(\theta_i-\theta_j)\big] - b_{ij}E_iE_j\sin(\theta_i-\theta_j), \tag{6}$$

where $\forall i,\ j \in \mathcal{S}_{\rm gen} \cup \mathcal{S}_{\rm load}$. $\mathcal{S}_{\rm line}$ denotes the set of power lines; E_i denotes voltage magnitude of the ith bus; g_{ij} and b_{ij} denote conductance and susceptance of line $(i,j) \in \mathcal{S}_{\rm line}$, respectively.

Conventionally, the value of P_i^0 in (3) is determined in an open-loop manner by solving economic dispatch problem periodically, and during each period, P_i^0 of the GUs participating in secondary frequency control are adjusted in a close-loop manner to bring the frequency deviation back to zero with the help of AGC.

In this paper, the distributed RTOPF control approach determines P_i^0 of each GU by exchanging information with its neighboring GU agents and sensor agents (as shown in Fig. 1). The control objective can be described as follows.

Firstly, the frequency deviation in all locations converges to zero in the steady state, i.e.,

$$\lim_{t\to\infty} \Delta\omega_i = 0, \ \forall i \in \{1, \cdots, n\}. \tag{7}$$

Secondly, the generation cost is minimized at the equilibrium, i.e., when (7) is attained, the control variables P_i^0 ($\forall i \in S_{\rm gen}$) converge to the optimal solution of the OPF problem as

$$\min_{\boldsymbol{P}_0} \ f(\boldsymbol{P}_0) = \sum_{i\in S_{\rm gen}} f_i(P_i^0) \tag{8a}$$

s.t.

$$P_{\rm load} + P_{\rm loss} - \sum_{i\in S_{\rm gen}} P_i^0 = 0 \tag{8b}$$

$$P_i^{\min} \le P_i^0 \le P_i^{\max}, \quad \forall i \in S_{\rm gen} \tag{8c}$$

$$F_{i,j} \le \bar{F}_{i,j}, \qquad \forall (i,j) \in S_{\rm line} \tag{8d}$$

The total generation cost $f(\boldsymbol{P}_0)$ in (8a) is to be minimized, where $\boldsymbol{P}_0 = [P_1^0, \cdots, P_q^0]^T$ is the decision vector. The cost of the ith GU $f_i(P)$ is a convex function, and without loss of generality, it is approximated as a quadratic function as [16]

$$f_i(P) = a_iP^2 + b_iP + c_i, \tag{9}$$

where a_i, b_i and c_i are cost coefficients.

Eq. (8b) is the power balance constraint, where $P_{\rm load}$ and $P_{\rm loss}$ are the aggregated load consumption and power loss. In this paper, we actually use $\Delta\omega_i$, which can be measured and calculated locally, as a feedback signal to reach power balance in the grid. This avoids the estimate of $P_{\rm load}$ and $P_{\rm loss}$ as did in [29]. The attainment of (7) actually indicates (8b), but eq. (8b) is still included here for the integrity of the OPF problem and the ease of illustrating the proposed approach in the next section. Eq. (8c) is the generation limit constraint of the ith GU ($\forall i \in S_{\rm gen}$), where $P_i^{\min}$ and $P_i^{\max}$ are the lower and upper bounds of its power output, respectively. Eq. (8d) is the power flow limit constraint of line (i,j) for all $(i,j) \in \mathcal{S}_{\rm line}$. $F_{i,j}$ and $\bar{F}_{i,j}$ are the actual power flow from bus i to j and its corresponding upper limit, respectively. There is no lower limit on $F_{i,j}$, such as $F_{i,j} > -\bar{F}_{i,j}$, since $F_{i,j}$ and $F_{j,i}$ are considered separately.

III. The Distributed RTOPF Control Approach

To make the OPF problem more tractable with real-time cooperative control and optimization, it is reformulated by including constraint (8d) in the objective function as a penalty term as [30]

$$\min_{\boldsymbol{P}_0} \ \tilde{f}(\boldsymbol{P}_0) = \sum_{i\in S_{\rm gen}} f_i(P_i^0) + \frac{1}{2}\gamma \sum_{(j,k)\in\mathcal{S}_{\rm line}} \{[F_{j,k} - \bar{F}_{j,k}]_+\}^2 \tag{10}$$

s.t. (8b) and (8c)

where $\gamma > 0$ is a predefined penalty factor, and the projection function is defined as

$$[x]_+ = \begin{cases} x & \text{if } x > 0 \\ 0 & \text{otherwise} \end{cases}.$$

By using the penalty method, power flow constraints (8d) may be slightly violated and the system may operate in a sub-optimal solution of the OPF problem (8). However, a trivial safety margin can always be reserved in the thermal limit of each power line. This margin can be kept sufficiently small by tuning the value of γ, which will not significantly degrade the optimality of the solution.

A. Centralized Solution to the RTOPF Problem

Define the Lagrangian function of the reformulated OPF problem as

$$\begin{aligned} L = f(\boldsymbol{P}_0) + \frac{1}{2}\gamma \sum_{(j,k)\in\mathcal{S}_{\text{line}}} \{[F_{j,k} - \bar{F}_{j,k}]_+\}^2 \\ + \lambda(P_{\text{load}} + P_{\text{loss}} - \sum_{i\in S_{\text{gen}}} P_i^0) \\ + \sum_{i\in S_{\text{gen}}} \nu_{i1}(P_i^0 - P_i^{\max}) \\ + \sum_{i\in S_{\text{gen}}} \nu_{i2}(P_i^{\min} - P_i^0), \end{aligned} \tag{11}$$

where λ, ν_{i1} and ν_{i2} ($\forall i \in S_{\text{gen}}$) are the Karush–Kuhn–Tucker (KKT) multipliers.

Lemma 1: $\boldsymbol{P}_0$ is the optimal solution of the OPF problem if it satisfies the KKT conditions as [30]

$$\begin{cases} P_i^0 = \dfrac{\lambda - b_i - \nu_{i1} + \nu_{i2} - \gamma \sum_{(j,k)\in S_{\text{line}}} [F_{j,k} - \bar{F}_{j,k}]_+ d_i^{jk}}{2a_i} & \text{(12a)} \\ \nu_{i1}(P_i^0 - P_i^{\max}) = 0, \quad \nu_{i2}(P_i^{\min} - P_i^0) = 0 & \text{(12b)} \\ P_i^{\min} \le P_i^0 \le P_i^{\max}, \quad \forall i \in S_{\text{gen}} & \text{(12c)} \\ \sum_{i\in S_{\text{gen}}} P_i^0 - P_{\text{load}} - P_{\text{loss}} = 0 & \text{(12d)} \\ \nu_{i1}, \nu_{i2} \ge 0, \quad \forall i \in S_{\text{gen}} & \text{(12e)} \end{cases}$$

where (12a) follows from $\partial L/\partial P_i^0 = 0$, and d_i^{jk} is equal to $\partial F_{j,k}/\partial P_{G,i}$.

It follows from KKT conditions (12a), (12b) and (12c) that

$$P_i^0 = \text{Sat}(P_i^{\text{cent}}, P_i^{\min}, P_i^{\max}), \tag{13}$$

where

$$P_i^{\text{cent}} = \frac{\lambda - b_i - \gamma \sum_{(j,k)\in\mathcal{S}_{\text{line}}} [F_{j,k} - \bar{F}_{j,k}]_+ d_i^{jk}}{2a_i},$$

is the centralized solution, and the saturation function is defined as

$$\text{Sat}(x, \min, \max) = \begin{cases} \min & \text{if } x < \min \\ \max & \text{if } x > \max \\ x & \text{otherwise} \end{cases}.$$

However, control law (13) cannot be implemented at any GU unless it can acquire global information to solve (12).

B. Distributed Solution to the RTOPF Problem

Inspired by (13), a distributed RTOPF control strategy is presented: the power generation set-point of the ith GU is controlled as

$$P_i^0 = \text{Sat}(P_i^{\text{dist}}, P_i^{\min}, P_i^{\max}), \tag{14}$$

where

$$P_i^{\text{dist}} = \frac{\lambda^{(i)} - b_i - \gamma \sum_{(j,k)\in\mathcal{S}_{\text{crit}}} \Delta F_{j,k}^{(i)} d_i^{jk}}{2a_i},$$

$\lambda^{(i)}$ is the estimate of λ, $\Delta F_{j,k}^{(i)}$ is the estimate of $[F_{j,k} - \bar{F}_{j,k}]_+$, and $\mathcal{S}_{\text{crit}} \subseteq \mathcal{S}_{\text{gen}}$ is the set of critical lines that are under potential risk of power flow limit violation.

In what follows, $\lambda^{(i)}$ and $\Delta F_{j,k}^{(i)}$ are to be calculated in a distributed manner, while d_i^{jk} is to be approximated locally so that (14) can be distributively implemented at each GU.

1) Distributed Estimation of λ: Frequency deviation $\Delta\omega_i$, which can be measured locally at each bus, is used as a feedback signal to drive the system to frequency stability. For the ith GU agent, its $\lambda^{(i)}$ evolves as

$$\dot{\lambda}^{(i)} = \sum_{j\in\mathcal{N}_i} w_{ij}(\lambda^{(j)} - \lambda^{(i)}) - \frac{1}{2a_i}\Delta\omega_i, \tag{15}$$

where $w_{ij} = w_{ji}$ is a positive communication weight gain if the ith and jth GU agents can communicate with each other, otherwise $w_{ij} = w_{ji} = 0$. The neighboring set of the ith GU agent $\mathcal{N}_i$ consists of all the GU agents that can communicate with it.

Intuitively, the first term in (15) intends to synchronize $\lambda^{(i)}$ for all $i \in \mathcal{S}_{\text{gen}}$ to a consensus, while the second term uses frequency deviation $\Delta\omega_i$ as a feedback mechanism to facilitate power balance (12d) of the system. It follows from (2) and (3) that $\Delta\omega_i < 0$ in the steady state indicates that $\sum_{i\in\mathcal{S}_{\text{gen}}} P_i^0$ is insufficient, thus $\lambda^{(i)}$ for all $i \in \mathcal{S}_{\text{gen}}$ need to be increased, and vice versa.

According to the cooperative control theory [17], the sufficient condition for $\lambda^{(i)}$ to converge to a consensus is that the communication network should be connected, i.e., there is a path between every pair of GU agents. Equivalently, the corresponding Laplacian matrix L defined as

$$[L]_{ij} = \begin{cases} -w_{ij} & \text{if } i \ne j \\ \sum_{l\ne i} w_{il} & \text{if } i = j \end{cases} \tag{16}$$

is irreducible.

2) Distributed Estimation of $[F_{j,k} - \bar{F}_{j,k}]_+$: Next, to calculate (14) in a distributed way, $[F_{j,k} - \bar{F}_{j,k}]_+$ for all $(j,k) \in \mathcal{S}_{\text{crit}}$ also needs to be known to each GU agent. This is achieved by making use of the abundant distributed sensor agents in the MAS. These sensors are installed at certain buses of the power system to measure the power flows of critical lines starting from the buses. The power flow limit $\bar{F}_{j,k}$ of each critical line is also stored at the corresponding sensor agent, so that $[F_{j,k} - \bar{F}_{j,k}]_+$ can be locally calculated. The simplest way is to broadcast $[F_{j,k} - \bar{F}_{j,k}]_+$ to all the GU agents directly so that $\Delta F_{j,k}^{(i)} \equiv [F_{j,k} - \bar{F}_{j,k}]_+$ for all $i \in \mathcal{S}_{\text{gen}}$.

Alternatively, each GU agents can also estimate $[F_{j,k} - \bar{F}_{j,k}]_+$ with the leader-following consensus algorithm [17]: to avoid long-distance communication, the information of $[F_{j,k} - \bar{F}_{j,k}]_+$ only needs to be transmitted to at least one neighboring GU agent (as exemplified in Fig. 1), the set of which is denoted as the leader set $\mathcal{L}_{j,k}$. To propagate the information of $[F_{j,k} - \bar{F}_{j,k}]_+$ to all the GU agents, the leader GU agents should fix their $\Delta F_{j,k}^{(i)}$ as

$$\Delta F_{j,k}^{(i)} \equiv [F_{j,k} - \bar{F}_{j,k}]_+, \quad \forall i \in \mathcal{L}_{j,k}, \tag{17}$$

while the follower GU agents should update their $\Delta F_{j,k}^{(i)}$ as

$$\Delta \dot{F}_{j,k}^{(i)} = g \sum_{l=1}^{q} w_{il} (\Delta F_{j,k}^{(l)} - \Delta F_{j,k}^{(i)}), \quad \forall i \in \mathcal{S}_{\text{gen}} - \mathcal{L}_{j,k}, \tag{18}$$

where $g > 0$ is a constant gain.

It follows from [17, Theorem 5.4] that $\Delta F_{j,k}^{(i)}$ for all $i \in \mathcal{S}_{\text{gen}}$ converge to $[F_{j,k} - \bar{F}_{j,k}]_+$.

Note that in a power system, only a small number of power lines might reach the power flow limits, otherwise the power grid needs upgrade. An off-line analysis can be executed on the grid to determine $\mathcal{S}_{\text{cirt}}$ and the corresponding location to install distributed sensors and communication devices. So as to save communication resource, the leader-following consensus (17) and (18) can stay idle when $[F_{j,k} - \bar{F}_{j,k}]_+ = 0$.

3) Local Calculation of d_i^{jk}: DC power flow is adopted due to its simplicity to locally estimate the value of d_i^{jk}. DC power flow is accurate enough in bulk power grids where $X/R \gg 0$ [31]. In islanded MV/HV micro-grids where the assumption $X/R \gg 0$ does not strictly hold, simulation result in Section IV-A shows that although the approximation of DC power flow could incur higher control error than that in bulk power grids, the result is acceptable to the micro-grid operator considering the fact that the conventional hierarchical control based upon load forecast can be costly and even less accurate. It should also be noted that in LV micro-grid ($X/R \ll 0$), the converged operating point could completely deviate from the OPF solution, which is unacceptable and subject to further investigation.

The DC power flow can be expressed as [4]:

$$[P_{e,1}, \cdots, P_{e,n}]^T = B[\theta_1, \cdots, \theta_n]^T, \tag{19}$$

$$F_{j,k} = -B_{jk}(\theta_j - \theta_k), \quad \forall (j,k) \in S_{\text{line}} \tag{20}$$

where $\mathcal{S}_{\text{line}}$ is the set of power lines, $F_{j,k}$ is the power flow from bus j to k, $B \in \mathbb{R}^{n \times n}$ is the susceptance matrix of the network, and is defined as

$$[B]_{ij} = \begin{cases} -b_{ij} & \text{if } i \neq j \\ \sum_{l \neq i} b_{il} & \text{if } i = j \end{cases},$$

thus $\text{rank}(B) = n - 1$.

Without loss of generality, suppose that the nth bus is the reference bus with $\theta_n = 0$. Eq. (19) can be reduced to

$$[P_{e,1}, \cdots, P_{e,n-1}]^T = \tilde{B}[\theta_1, \cdots, \theta_{n-1}]^T, \tag{21}$$

where $\tilde{B} \in \mathbb{R}^{(n-1)\times(n-1)}$ equals the susceptance matrix B excluding the nth column and row, and $\text{rank}(\tilde{B}) = n - 1$.

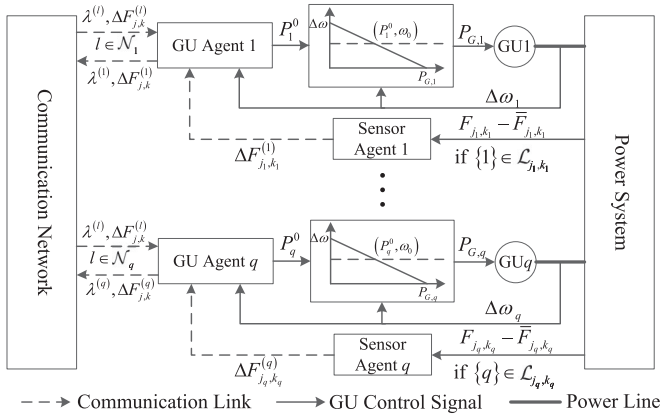

Fig. 2. Architecture of the distributed RTOPF control approach

Pre-multiplying the two sides of (21) by $\tilde{B}^{-1}$ leads to

$$[\theta_1, \cdots, \theta_{n-1}]^T = \tilde{B}^{-1}[P_1, \cdots, P_{n-1}]^T. \tag{22}$$

Therefore,

$$\frac{\partial \theta_i}{\partial P_{e,j}} = \begin{cases} [\tilde{B}^{-1}]_{ij} & \text{if } j \neq n \\ 0 & \text{otherwise} \end{cases} \tag{23}$$

It follows from eqs. (20) and (23) that d_i^{jk} can be approximated as

$$d_i^{jk} = \begin{cases} -B_{jk}([\tilde{B}^{-1}]_{ji} - [\tilde{B}^{-1}]_{ki}) & \text{if } i \neq n \\ 0 & \text{otherwise} \end{cases}. \tag{24}$$

It should be noted that, to estimate d_i^{jk} locally at each GU, the information of matrix B needs to be stored in all the GU agents. Once the structure of the power grid changes, matrix B can be updated in a peer-to-peer fashion.

C. Main Result

Fig. 2 is the architecture of the distributed RTOPF control approach, which shows the flow of information in the MAS. The convergence property of the proposed distributed RTOPF control approach can be summarized as the following theorem.

Theorem 1: Assume that the communication network among the GU agents is connected. The power output of each GU is determined by the frequency droop control (3), where the power set-point is determined by the distributed control law in Section III-B. This networked control system is Lyapunov stable. In the steady state, the frequency deviation is removed and the system's operational point converges to a sub-optimal solution of the OPF problem (8).

The proof of the theorem is provided in Appendix A. It should be noted that the proof of convergence is based on linearized AC power flow, thus it holds for both islanded micro-grid and bulk power grid.

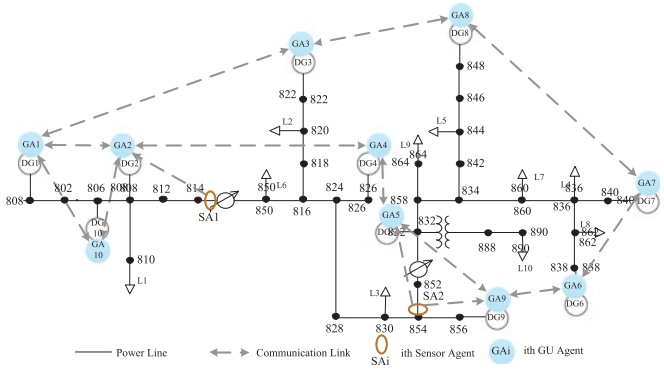

Fig. 3. Control scheme of the IEEE 34-bus islanded micro-grid.

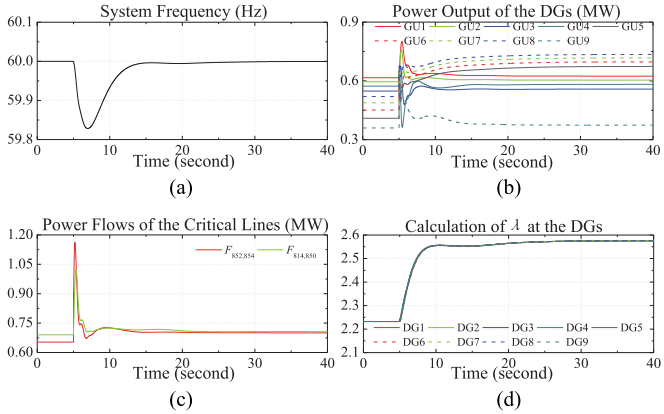

Fig. 4. System response to random power disturbance.

IV. Simulation Results

In this section, the proposed distributed RTOPF control approach is validated in an islanded micro-grid modified from the IEEE 34-bus test feeder and the IEEE 118-bus bulk power grid with DIgSILENT PowerFactory. The steady-state results are compared with AC OPF results calculated by MATPOWER [32] to demonstrate the accuracy of the proposed approach.

A. IEEE 34-Bus Islanded Micro-Grid

When there is a fault in the main grid, the IEEE 34-bus test feeder can disconnect from it at Bus 800 and operate as a micro-grid in the islanded mode. The micro-grid has its main voltage at 24.9 kV. The single-line diagram with the overlaid communication network and distributed sensors are shown in Fig. 3. This islanded micro-grid comprises 10 DGs, with DG 10 initially remaining inactive to demonstrate the flexibility and scalability of the proposed approach. The key parameters of these DGs are shown in Table V in Appendix B. The micro-grid also includes 10 loads, namely L1-L10, with L10 initially disconnected from the grid to test response of the proposed approach under power disturbance. These loads are all modeled as constant power load. The power consumption of L1-L9 is 0.5 MW + 0.1 Mvar, while that for L10 is 1.0 MW + 0.1 Mvar. Power lines $(814, 850)$ and $(854, 852)$ are selected as the critical lines through off-line analysis. Their thermal limits are 0.8 MW and 0.7 MW, respectively. Reserving a trivial safety margin of 0.002 MW for each critical lines, i.e., $\bar{F}_{814,850} =$ 0.798 MW and $\bar{F}_{854,852} =$ 0.698 MW. Initially, all the DGs operate in the steady state, with constraints (8c) and (8d) remaining inactive.

First, the response of the networked control system to random power disturbance is studied: at $t = 5$ s, L10 is connected to the islanded micro-grid from Bus 890. The system response is shown in Fig. 4. Right after the load connection, because more active power is consumed than generated, the system frequency decreases to 59.83 Hz, as shown in Fig. 4(a). With the feedback of frequency error, each DG increases its $\lambda^{(i)}$ and thus its active power to rebalance the demand. Consequently, the system frequency is recovered to the nominal value 60 Hz after 15 s. Fig. 4(d) shows that the response of $\lambda^{(i)}$ for each DG almost coincides with each other during the transient. This is because the "force of consensus" outweighs the "force of feedback". Fig. 4(c) shows that after a new steady state is reached, the power flow of line $(854, 852)$ is saturated at 0.6981 MW. In the new steady state, the converged power outputs of DGs (as depicted in Fig. 4(b)) are compared with the ideal AC OPF result (no load forecast error is considered), as shown in Table I. It can be observed that the relative error is within 4.7%, which is satisfactory enough considering the fact that 1) in the real implementation of the hierarchical control, inaccurate load forecast could also introduce comparable or even more significant error and 2) load forecast in a micro-grid can be costly.

TABLE I
Comparison of the Simulation Results After Load Disturbance

DG No.	AC OPF (MW)	Proposed Approach (MW)	Relative Error (%)
1	0.595	0.623	4.71
2	0.586	0.604	3.07
3	0.556	0.558	0.36
4	0.587	0.582	−0.85
5	0.672	0.674	0.30
6	0.694	0.697	0.93
7	0.715	0.717	0.43
8	0.730	0.735	0.93
9	0.389	0.374	−3.86

Next, it is demonstrated that the proposed approach can make DGs plug-and-play: at $t = 5$ s, DG 10 is connected to the islanded micro-grid from Bus 806. The system response is shown in Fig. 5. The system converges to a new steady state in about 30 s. After DG 10 is plugged in, it gradually picks up load, and consequently results in power congestion of the two critical lines. Moreover, because the number of DGs increases, the power output of DG 1 - DG 9 can slightly decrease, so does the consensus of $\lambda^{(i)}$, as can be seen in Fig. 5(b) and (d). Table II compares the converged power outputs of DGs in the new steady state with the ideal AC OPF result. The maximum relative error is 5.0% in this case.

Third, the response of the proposed approach to time-varying generation limits is studied: at $t = 0$ s, $P_1^{\max}$ and $P_2^{\max}$ start to decrease from 0.7 MW to 0.4 MW at a rate of 0.02 MW/s due to

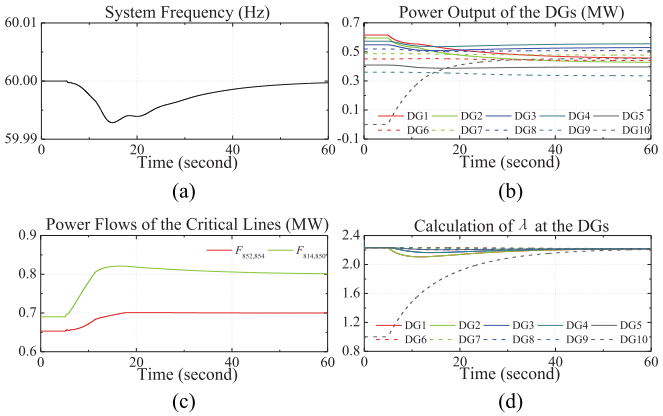

Fig. 5. System response to activation of DG 10.

TABLE II
COMPARISON OF THE SIMULATION RESULTS AFTER DG PLUG-IN

DG No.	AC OPF (MW)	Proposed Approach (MW)	Relative Error (%)
1	0.442	0.454	2.71
2	0.427	0.426	−0.23
3	0.504	0.525	4.17
4	0.537	0.556	3.54
5	0.399	0.397	−0.50
6	0.452	0.440	−2.65
7	0.488	0.478	−2.09
8	0.517	0.511	−1.16
9	0.319	0.335	5.02
10	0.443	0.453	2.26

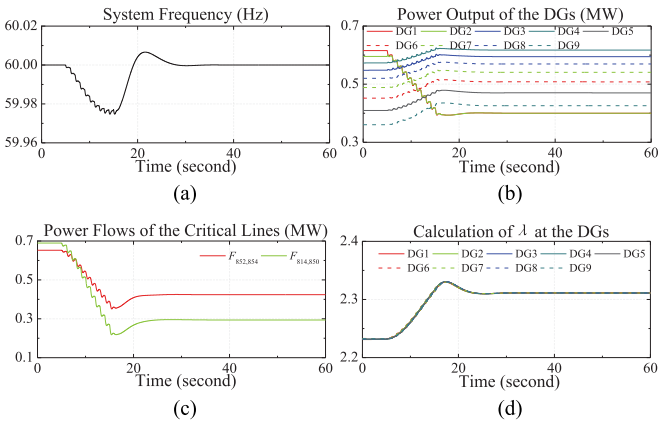

Fig. 6. System response to time-varying generation limits.

the change of weather condition. The system response is shown in Fig. 6. As can be observed from Fig. 6(b), generation limits of DG 1 and DG 2 become active constraints at $t = 5$ s. The other DGs should increase their power output to maintain the power balance within the grid. To demonstrate the robustness of the proposed approach to communication interruption, communication between DG 5 and DG 9 is blocked since $t = 5$ s. To adapt to this change, DG 5 and DG 9 set the corresponding weights w_{59} and w_{95} to 0 in (15) and (18). Since the resulting communication remains connected, convergence is still achieved. In

TABLE III
COMPARISON OF THE SIMULATION RESULTS UNDER TIME-VARYING GENERATION LIMITS

DG No.	AC OPF (MW)	Proposed Approach (MW)	Relative Error (%)
1	0.400	0.400	0.00
2	0.400	0.400	0.00
3	0.575	0.595	3.48
4	0.604	0.616	1.99
5	0.476	0.470	−1.26
6	0.520	0.508	−2.31
7	0.552	0.541	−1.99
8	0.577	0.570	−1.21
9	0.408	0.426	4.41
10	0.443	0.453	2.26

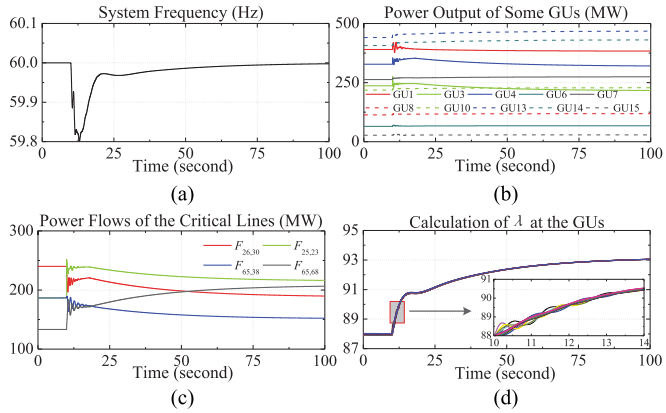

Fig. 7. Response of the IEEE 118-bus test system.

the new steady state, no critical line has reached the thermal limit. Table III compares the converged power outputs of DGs with the ideal AC OPF result. The relative error is within 4.4% in this case.

B. IEEE 118-Bus System

The proposed approach is also tested in a bulk power grid. The IEEE 118-bus test case represents a simple approximation of the American Electric Power System in the U.S. Midwest, which contains 172 buses, 185 transmission lines, 76 transformers and 91 constant power loads. Detailed parameters of the grid can be found in the MATPOWER case file 'case118'. 19 GUs are connected to the grid from different locations, the key parameters of which are shown in Table VI in Appendix B. The corresponding GU agents are interconnected with a ring-shape communication network in ascending order of their numbers. The parameters of 4 critical power lines are shown in Table VII in Appendix B. An 1 MW safety margin is reserved for each critical line.

Initially, all the GUs operate in the steady state, with only thermal limit constraint of line (26, 30) being active. At $t =$ 10 s, the load at Bus 23 increases from 7 MW to 140 MW to imitate a severe power disturbance. The response of the system is depicted in Fig. 7. It can be observed that the system converges in about 90 s, which is slower than that in the islanded

TABLE IV
COMPARISON OF THE RESULT IN THE IEEE 118-BUS SYSTEM

GU No.	AC OPF (MW)	Proposed Approach (MW)	Relative Error (%)
1	379.0	382.9	1.03
2	152.4	146.8	−3.67
3	223.7	215.6	−3.62
4	331.3	319.8	−3.47
5	51.7	49.8	−3.67
6	67.7	67.9	0.30
7	273.2	275.5	0.08
8	121.6	119.1	−2.06
9	220.9	221.7	0.36
10	223.6	228.7	2.28
11	339.5	349.5	2.95
12	338.2	348.5	3.05
13	452.7	468.1	3.40
14	426.6	431.1	1.05
15	28.7	28.8	0.35
16	365.2	364.9	−0.6
17	259.1	258.7	−0.15
18	98.9	97.6	−1.31
19	89.0	89.3	0.34

micro-grid. This is partly because there are more GUs in this grid, and GUs in a bulk power grid have higher inertia constants. In the transient, the system frequency declines to 59.8 Hz before recovering the nominal value. Because the dynamics of the distributed RTOPF approach reacts relatively slowly, the transient behavior is mainly influenced by the droop constant k_{Di}, thus the transient performance is comparable to that of the primary frequency control. After convergence, Fig. 7(b) shows that the GUs are still within their full capacities, while Fig. 7(c) shows that only power flow of line (25, 23) exceeds $\bar{F}_{25,23}$ by about 0.8 MW. Thus the power flow is still within its thermal limit. The result of the proposed control approach is compared with that of the ideal AC OPF in Table IV , which shows that the maximum relative error is within 3.7%. This relative error is smaller than that in the islanded micro-grid mainly because DC power flow is more accurate in a bulk power grid.

V. CONCLUSION

A multi-agent system based distributed real-time optimal power flow control approach, which integrates the function of the conventional hierarchical control, is proposed in this paper. By means of distributively measuring power flow and system frequency, and exchanging a minimum amount of information among neighboring GU agents, the proposed strategy can recover the nominal frequency, while minimize the generation cost of the GUs in real time under power balance, generation limit, and power flow limit constraints. The proposed strategy is economically efficient in comparison with the conventional hierarchical scheme, where load forecast inaccuracy and relatively slow updating period of tertiary control could incur higher control error. Moreover, it is robust to communication interruption and can meet the requirement of plug-and-play. Simulation results based on an islanded micro-grid modified from the IEEE 34-bus test feeder and the IEEE 118-bus bulk power grid demonstrate the effectiveness and accuracy of the proposed approach.

APPENDIX A
PROOF OF THEOREM 1

The proof of Theorem 1 can be proceeded in two steps.

Step 1: Linearization

Linearizing eqs. (4) and (5) around a stable operational point (denoted with $*$ superscript) leads to

$$\Delta P_{e,i} = \sum_{(i,j)\in\mathcal{S}_{\text{line}}} \beta_{ij}^p(\Delta\theta_i - \Delta\theta_j) + \epsilon_{ij,1}^p \Delta E_i + \epsilon_{ij,2}^p \Delta E_j, \tag{25}$$

$$\Delta Q_{e,i} = \sum_{(i,j)\in\mathcal{S}_{\text{line}}} \beta_{ij}^q(\Delta\theta_i - \Delta\theta_j) + \epsilon_{ij,1}^q \Delta E_i + \epsilon_{ij,2}^q \Delta E_j, \tag{26}$$

where $\Delta x = x - x^*$ with x being any variables, and

$$\begin{aligned}
\beta_{ij}^p &= E_i^* E_j^* [b_{ij}\cos(\theta_i^* - \theta_j^*) - g_{ij}\sin(\theta_i^* - \theta_j^*)],\\
\epsilon_{ij,1}^p &= E_j^* [g_{ij}\cos(\theta_i^* - \theta_j^*) - b_{ij}\sin(\theta_i^* - \theta_j^*)],\\
\epsilon_{ij,2}^p &= E_i^* [g_{ij}\cos(\theta_i^* - \theta_j^*) - b_{ij}\sin(\theta_i^* - \theta_j^*)],\\
\beta_{ij}^q &= E_i^* E_j^* [g_{ij}\cos(\theta_i^* - \theta_j^*) - b_{ij}\sin(\theta_i^* - \theta_j^*)],\\
\epsilon_{ij,1}^q &= E_j^* [g_{ij}\sin(\theta_i^* - \theta_j^*) - b_{ij}\cos(\theta_i^* - \theta_j^*)],\\
\epsilon_{ij,2}^q &= E_i^* [g_{ij}\sin(\theta_i^* - \theta_j^*) - b_{ij}\cos(\theta_i^* - \theta_j^*)].
\end{aligned}$$

Compactly, eqs. (25) and (26) can be written as

$$\begin{bmatrix}\Delta \boldsymbol{P}_{e,G}\\ \Delta \boldsymbol{P}_{e,L}\end{bmatrix} = \overbrace{\begin{bmatrix}\mathcal{B}_{GG}^p & \mathcal{B}_{GL}^p\\ \mathcal{B}_{LG}^p & \mathcal{B}_{LL}^p\end{bmatrix}}^{\mathcal{B}^p}\begin{bmatrix}\Delta\boldsymbol{\theta}_G\\ \Delta\boldsymbol{\theta}_L\end{bmatrix} + \underbrace{\begin{bmatrix}\mathcal{E}_{GG}^p & \mathcal{E}_{GL}^p\\ \mathcal{E}_{LG}^p & \mathcal{E}_{LL}^p\end{bmatrix}}_{\mathcal{E}^p}\begin{bmatrix}\Delta\boldsymbol{E}_G\\ \Delta\boldsymbol{E}_L\end{bmatrix}, \tag{27}$$

$$\begin{bmatrix}\Delta \boldsymbol{Q}_{e,G}\\ \Delta \boldsymbol{Q}_{e,L}\end{bmatrix} = \overbrace{\begin{bmatrix}\mathcal{B}_{GG}^q & \mathcal{B}_{GL}^q\\ \mathcal{B}_{LG}^q & \mathcal{B}_{LL}^q\end{bmatrix}}^{\mathcal{B}^q}\begin{bmatrix}\Delta\boldsymbol{\theta}_G\\ \Delta\boldsymbol{\theta}_L\end{bmatrix} + \underbrace{\begin{bmatrix}\mathcal{E}_{GG}^q & \mathcal{E}_{GL}^q\\ \mathcal{E}_{LG}^q & \mathcal{E}_{LL}^q\end{bmatrix}}_{\mathcal{E}^q}\begin{bmatrix}\Delta\boldsymbol{E}_G\\ \Delta\boldsymbol{E}_L\end{bmatrix}, \tag{28}$$

where $\Delta\boldsymbol{P}_{e,G} = [\Delta P_{e,1}, \cdots, \Delta P_{e,q}]^T$, $\Delta\boldsymbol{P}_{e,L} = [\Delta P_{e,q+1}, \cdots, \Delta P_{e,n}]^T$, $\Delta\boldsymbol{Q}_{e,G} = [\Delta Q_{e,1}, \cdots, \Delta Q_{e,q}]^T$, $\Delta\boldsymbol{Q}_{e,L} = [\Delta Q_{e,q+1}, \cdots, \Delta Q_{e,n}]^T$, $\Delta\boldsymbol{\theta}_G = [\Delta\theta_1, \cdots, \Delta\theta_q]^T$, $\Delta\boldsymbol{\theta}_L = [\Delta\theta_{q+1}, \cdots, \Delta\theta_n]^T$, $\Delta\boldsymbol{E}_G = [\Delta E_1, \cdots, \Delta E_q]^T$, $\Delta\boldsymbol{E}_L = [\Delta E_{q+1}, \cdots, \Delta E_n]^T$, and

$$[\mathcal{B}^s]_{ij} = \begin{cases} -\beta_{ij}^s & \text{if } i \neq j\\ \sum_{l\neq i}\beta_{il}^s & \text{if } i = j\end{cases},$$

$$[\mathcal{E}^s]_{ij} = \begin{cases} \epsilon_{ij,2}^s & \text{if } i \neq j\\ \sum_{l\neq i}\epsilon_{ij,1}^s & \text{if } i = j\end{cases},$$

with s being p or q.

For the GU buses, consider the corresponding voltages are controlled constant (PV node), i.e., $\Delta \boldsymbol{E}_G = 0$; for the Load buses, consider the corresponding active/reactive power injections are controlled constant (PQ node), i.e., $\Delta \boldsymbol{P}_{e,L} = 0$ and $\Delta \boldsymbol{Q}_{e,L} = 0$. It follows from (28) that

$$\Delta E_L = -(\mathcal{E}^p_{LL})^{-1}(\mathcal{B}^q_{LG}\Delta\theta_G + \mathcal{B}^q_{LL}\theta_L) \tag{29}$$

Substituting (29) into (27) leads to

$$\begin{bmatrix} \Delta \boldsymbol{P}_{e,G} \\ \Delta \boldsymbol{P}_{e,L} \end{bmatrix} = \underbrace{\begin{bmatrix} \mathcal{B}_{GG} & \mathcal{B}_{GL} \\ \mathcal{B}_{LG} & \mathcal{B}_{LL} \end{bmatrix}}_{\mathcal{B}} \begin{bmatrix} \Delta \boldsymbol{\theta}_G \\ \Delta \boldsymbol{\theta}_L \end{bmatrix}, \tag{30}$$

where

$$\mathcal{B} = \begin{bmatrix} \mathcal{B}^p_{GG} - \mathcal{E}^p_{GL}(\mathcal{E}^q_{LL})^{-1}\mathcal{B}^q_{LG} & \mathcal{B}^p_{GL} - \mathcal{E}^p_{GL}(\mathcal{E}^q_{LL})^{-1}\mathcal{B}^q_{LL} \\ \mathcal{B}^p_{LG} - \mathcal{E}^p_{LL}(\mathcal{E}^q_{LL})^{-1}\mathcal{B}^q_{LG} & \mathcal{B}^p_{LL} - \mathcal{E}^p_{LL}(\mathcal{E}^q_{LL})^{-1}\mathcal{B}^q_{LL} \end{bmatrix}.$$

It can be inferred from (30) that

$$\Delta \boldsymbol{\theta}_L = -\mathcal{B}^{-1}_{LL}\mathcal{B}_{LG}\Delta\boldsymbol{\theta}_G, \tag{31}$$

which can lead to

$$\Delta \boldsymbol{P}_{e,G} = (\mathcal{B}_{GG} - \mathcal{B}_{GL}\mathcal{B}^{-1}_{LL}\mathcal{B}_{LG})\Delta\boldsymbol{\theta}_G \triangleq (\mathcal{B}_r + \Delta\mathcal{B}_r)\Delta\boldsymbol{\theta}_G, \tag{32}$$

The coefficient matrix $\mathcal{B}_{GG} - \mathcal{B}_{GL}\mathcal{B}^{-1}_{LL}\mathcal{B}_{LG}$ can always be decomposed as $\mathcal{B}_r + \Delta\mathcal{B}_r$, where $\mathcal{B}_r$ is an irreducible and symmetrical Laplacian matrix, and $\Delta\mathcal{B}_r$ can be viewed as a perturbation. Furthermore, it can be verified through numerical analysis that $\Delta\mathcal{B}_r$ is close to all-zero matrix. Ignoring the high-order infinitesimal, (32) can be simplified as

$$\Delta \boldsymbol{P}_{e,G} = \mathcal{B}_r \Delta \boldsymbol{\theta}_G. \tag{33}$$

Linearizing eq. (6) around a stable operational point leads to

$$\Delta F_{i,j} = \beta^f_{ij}(\Delta\theta_i - \Delta\theta_j) + \epsilon^f_{ij,1}\Delta E_i + \epsilon^f_{ij,2}\Delta E_j, \tag{34}$$

where

$$\beta^f_{ij} = E^*_i E^*_j[g_{ij}\sin(\theta^*_i - \theta^*_j) - b_{ij}\cos(\theta^*_i - \theta^*_j)],$$

$$\epsilon^f_{ij,1} = 2g_{ij}E^*_i - g_{ij}E^*_j\cos(\theta^*_i - \theta^*_j) - b_{ij}E^*_j\sin(\theta^*_i - \theta^*_j),$$

$$\epsilon^f_{ij,2} = -g_{ij}E^*_i\cos(\theta^*_i - \theta^*_j) - b_{ij}E^*_i\sin(\theta^*_i - \theta^*_j).$$

By invoking eqs. (29) and (31), eq. (34) leads to

$$\Delta F_{i,j} = \boldsymbol{\phi}^T_{i,j}\Delta\boldsymbol{\theta}_G, \tag{35}$$

where the expression of $\boldsymbol{\phi}_{i,j} \in \mathbb{R}^q$ can be easily inferred thus is omitted here due to the limit of space.

Step 2: Lyapunov Stability Analysis

Consider that the optimal solution of the reformulated OPF problem (10) (denoted with $*$ superscript) satisfies

$$\begin{aligned} \boldsymbol{P}^*_0 &\triangleq [P^{0*}_1, \cdots, P^{0*}_q]^T \\ &= \text{vec}\left\{\frac{\lambda^* - b_i - \gamma\sum_{(j,k)\in\mathcal{S}_{\text{crit}}}[F^*_{j,k} - \bar{F}_{j,k}]_+ d^{jk}_i}{2a_i}\right\} \end{aligned} \tag{36}$$

where vec$\{x_i\}$ denotes a vector of proper size with its ith entry equal to x_i.

It follows from the analysis in *Step 1* that $\mathcal{B}_r$ is an irreducible and symmetrical Laplacian matrix. Thus rank$(\mathcal{B}_r) = q - 1$ and $\boldsymbol{\theta}^*_G$ is undetermined, i.e., if $\boldsymbol{\theta}^*_G = \boldsymbol{\theta}_0$ satisfies (36), $\boldsymbol{\theta}^*_G = \boldsymbol{\theta}_0 + \mathbf{1}_q c$ also does for all $c \in \mathbb{R}$, where $\mathbf{1}_q \in \mathbb{R}^q$ is an all-one vector. In the following analysis, $\boldsymbol{\theta}^*_G$ is selected so that

$$\mathbf{1}^T_q \Delta\boldsymbol{\theta}_G = \mathbf{1}^T_q\boldsymbol{\theta}_G - \mathbf{1}^T_q\boldsymbol{\theta}^*_G \equiv 0. \tag{37}$$

Thus $\mathbf{1}^T_q\dot{\boldsymbol{\theta}}^*_G = \mathbf{1}^T_q\dot{\boldsymbol{\theta}}_G = \mathbf{1}^T_q\Delta\boldsymbol{\omega}$, where $\Delta\boldsymbol{\omega} = [\Delta\omega_1, \cdots, \Delta\omega_q]^T$. Since the changing rate of θ^*_i is the same for all $i \in \mathcal{S}_{\text{gen}}$, $\dot{\boldsymbol{\theta}}^*_G = \frac{1}{q}\mathbf{1}_{q\times q}\Delta\boldsymbol{\omega}$, where $\mathbf{1}_{q\times q} \in \mathbb{R}^{q\times q}$ is an all-one matrix.

It follows from (14), (33) and (36) that (2) can be rewritten in the compact form as

$$\begin{aligned} T\Delta\dot{\boldsymbol{\omega}} &= \Delta\boldsymbol{P}_G - \Delta\boldsymbol{P}_{e,G} = \Delta\boldsymbol{P}_0 - K_D\Delta\boldsymbol{\omega} - \Delta\boldsymbol{P}_{e,G} \\ &= -\mathcal{B}_r\Delta\boldsymbol{\theta}_G + \Lambda\Delta\boldsymbol{\lambda} - K_D\Delta\boldsymbol{\omega} - \Lambda\Delta\boldsymbol{F} \end{aligned}, \tag{38}$$

where $\Delta\boldsymbol{\lambda} = [\lambda^{(1)} - \lambda^*, \cdots, \lambda^{(q)} - \lambda^*]^T$, $K_D = \text{diag}\{[k_{D1}, \cdots, k_{Dq}]\}$, $T = \text{diag}\{[T_1, \cdots, T_q]\}$, $\Lambda = \text{diag}\{[\frac{1}{2a_1}, \cdots, \frac{1}{2a_q}]\}$, and

$$\Delta\boldsymbol{F} = \gamma\text{vec}\left\{\sum_{(j,k)\in\mathcal{S}_{\text{crit}}} d^{jk}_i([F_{j,k} - \bar{F}_{j,k}]_+ - [F^*_{j,k} - \bar{F}_{j,k}]_+)\right\}$$

Therefore, the dynamics of the error system can be characterized as

$$\begin{bmatrix} \Delta\dot{\boldsymbol{\theta}}_G \\ \Delta\dot{\boldsymbol{\omega}} \\ \Delta\dot{\boldsymbol{\lambda}} \end{bmatrix} = \begin{bmatrix} 0 & I_q - \frac{1}{q}\mathbf{1}_{q\times q} & 0 \\ -T^{-1}\mathcal{B}_r & -T^{-1}K_D & T^{-1}\Lambda \\ 0 & -\Lambda & -L \end{bmatrix} \begin{bmatrix} \Delta\boldsymbol{\theta}_G \\ \Delta\boldsymbol{\omega} \\ \Delta\boldsymbol{\lambda} \end{bmatrix} + \begin{bmatrix} 0 \\ -T^{-1}\Lambda\Delta\boldsymbol{F} \\ 0 \end{bmatrix} \tag{39}$$

where $L \in \mathbb{R}^{q\times q}$ is the graph Laplacian of the communication network defined in (16).

Choose a Lyapunov candidate as

$$\begin{aligned} V = {} & \alpha\Delta\boldsymbol{\theta}^T_G\mathcal{B}_r\Delta\boldsymbol{\theta} + \alpha\Delta\boldsymbol{\omega}^T T\Delta\boldsymbol{\omega} \\ & + \alpha\Delta\boldsymbol{\lambda}^2 + \Delta\boldsymbol{\theta}^T_G T\Delta\boldsymbol{\omega} - \beta\Delta\boldsymbol{\lambda}^T T\Delta\boldsymbol{\omega}. \end{aligned} \tag{40}$$

Define a state transformation matrix $T_B = [\boldsymbol{\nu}_{B1}, N_B]^T$, where $N_B = [\boldsymbol{\nu}_{B2}, \cdots, \boldsymbol{\nu}_{Bq}]$ and $\boldsymbol{\nu}_{Bi}$ is the left eigenvector corresponding to the ith eigenvalue of $\mathcal{B}_r$, i.e., $\lambda_i(\mathcal{B}_r)$ for all $i \in \mathcal{S}_{\text{gen}}$. Specifically, $\mathcal{B}_r$ has a simple eigenvalue $\lambda_1(\mathcal{B}_r) = 0$ with its corresponding left eigenvector $\boldsymbol{\nu}_{B1} = \mathbf{1}_q$ since it is a symmetrical and irreducible Laplacian matrix [17]. Consider (37) and apply the state transformation to $\Delta\boldsymbol{\theta}_G$ as $T_B\Delta\boldsymbol{\theta}_G = [0, \delta\boldsymbol{\theta}^T_G]^T \Rightarrow \Delta\boldsymbol{\theta}_G = N_B\delta\boldsymbol{\theta}_G$, where $\delta\boldsymbol{\theta}_G \in \mathbb{R}^{q-1}$ is the transformed state vector. Thus eq. (40) can be rewritten as

$$\begin{aligned} V = {} & \alpha\delta\boldsymbol{\theta}^T_G\mathcal{B}'_r\delta\boldsymbol{\theta}_G + \alpha\Delta\boldsymbol{\omega}^T T\Delta\boldsymbol{\omega} + \alpha\Delta\boldsymbol{\lambda}^2 \\ & + \delta\boldsymbol{\theta}^T_G N^T_B T\Delta\boldsymbol{\omega} - \beta\Delta\boldsymbol{\lambda}^T_G T\Delta\boldsymbol{\omega}, \end{aligned}$$

where $\mathcal{B}_r' = N_B^T \mathcal{B}_r N_B = \text{diag}\{[\lambda_2(\mathcal{B}_r), \cdots, \lambda_q(\mathcal{B}_r)]\}$ is positive definite. Therefore, it follows from inequality $\|\boldsymbol{a}\|^2 + \|\boldsymbol{b}\|^2 \geq 2\boldsymbol{a}^T\boldsymbol{b}$ that V is positive definite for relatively large α.

The time derivative of the Lyapunov function in (40) along the trajectory of (39) can be calculated as

$$\begin{aligned}
\dot{V} = & \cancel{2\alpha\Delta\boldsymbol{\theta}_G^T\mathcal{B}_r\Delta\boldsymbol{\omega}} - \cancel{2\alpha\Delta\boldsymbol{\theta}_G^T\mathcal{B}_r\Delta\boldsymbol{\omega}} - 2\alpha\Delta\boldsymbol{\omega}^T K_D\Delta\boldsymbol{\omega} \\
& + \cancel{2\alpha\Delta\boldsymbol{\omega}^T\Lambda\Delta\boldsymbol{\lambda}} - 2\alpha\Delta\boldsymbol{\omega}^T\Lambda\Delta\boldsymbol{F} - \cancel{2\alpha\Delta\boldsymbol{\lambda}^T\Lambda\Delta\boldsymbol{\omega}} \\
& - 2\alpha\Delta\boldsymbol{\lambda}^T L\Delta\boldsymbol{\lambda} - \Delta\boldsymbol{\theta}_G^T\mathcal{B}_r\Delta\boldsymbol{\theta}_G - \Delta\boldsymbol{\theta}_G^T K_D\Delta\boldsymbol{\omega} \\
& + \Delta\boldsymbol{\theta}_G^T\Lambda\Delta\boldsymbol{\lambda} - \Delta\boldsymbol{\theta}_G^T\Lambda\Delta\boldsymbol{F} + \Delta\boldsymbol{\omega}^T T\left(I_q - \frac{1}{q}\mathbf{1}_{q\times q}\right)\Delta\boldsymbol{\omega} \\
& + \beta\Delta\boldsymbol{\lambda}^T\mathcal{B}_r\Delta\boldsymbol{\theta}_G + \beta\Delta\boldsymbol{\lambda}^T K_D\Delta\boldsymbol{\omega} - \beta\Delta\boldsymbol{\lambda}^T\Lambda\Delta\boldsymbol{\lambda} \\
& + \beta\Delta\boldsymbol{\lambda}^T\Lambda\Delta\boldsymbol{F} + \beta\Delta\boldsymbol{\omega}^T T\Lambda\Delta\boldsymbol{\omega} + \beta\Delta\boldsymbol{\omega}^T TL\Delta\boldsymbol{\lambda} \\
= & - \Delta\boldsymbol{\theta}_G^T\mathcal{B}_r\Delta\boldsymbol{\theta}_G - \Delta\boldsymbol{\omega}^T M_1\Delta\boldsymbol{\omega} - \Delta\boldsymbol{\lambda}^T(2\alpha L + \beta\Lambda)\Delta\boldsymbol{\lambda} \\
& - \Delta\boldsymbol{\theta}_G^T K_D\Delta\boldsymbol{\omega} + \Delta\boldsymbol{\theta}_G^T(\Lambda + \beta\mathcal{B}_r)\Delta\boldsymbol{\lambda} \\
& + \beta\Delta\boldsymbol{\lambda}^T(K_D + LT)\Delta\boldsymbol{\omega} - 2\alpha\Delta\boldsymbol{\omega}^T\Lambda\Delta\boldsymbol{F} \\
& - \Delta\boldsymbol{\theta}_G^T\Lambda\Delta\boldsymbol{F} + \beta\Delta\boldsymbol{\lambda}^T\Lambda\Delta\boldsymbol{F} \qquad (41)
\end{aligned}$$

where $M_1 = 2\alpha K_D - \beta T\Lambda - T(I_q - \frac{1}{q}\mathbf{1}_{q\times q}) \in \mathbb{R}^{q\times q}$.

Next, the upper bounds of its last three terms are derived with respect to the states in (39). The upper bound of the first term is derived in (42) as shown at the bottom of this page, where $\boldsymbol{d}_{jk} \triangleq [d_1^{jk}, \cdots, d_q^{jk}]^T$, and the symbol '$\wedge$' means to take the absolute value element-wise of the corresponding vector or matrix. The inequality follows from $|a| - |b| \leq |a - b|$ and (35). It can also be derived that $-\Delta\boldsymbol{\theta}_G^T\Lambda\Delta\boldsymbol{F} \leq \gamma\Delta\hat{\boldsymbol{\theta}}_G^T R_2\Delta\hat{\boldsymbol{\theta}}_G$ and $\beta\Delta\boldsymbol{\lambda}^T\Lambda\Delta\boldsymbol{F} \leq \gamma\beta\Delta\hat{\boldsymbol{\lambda}}^T R_3\Delta\hat{\boldsymbol{\theta}}_G$, where the expressions of R_2 and R_3 can be calculated similarly as in (42). Substituting the above inequalities into (41) leads to

$$\begin{aligned}
\dot{V} \leq & - \Delta\boldsymbol{\theta}_G^T\mathcal{B}_r\Delta\boldsymbol{\theta}_G + \gamma\Delta\hat{\boldsymbol{\theta}}_G^T R_2\Delta\hat{\boldsymbol{\theta}}_G - \Delta\boldsymbol{\omega}^T M_1\Delta\boldsymbol{\omega} \\
& - \Delta\boldsymbol{\lambda}^T(2\alpha L + \beta\Lambda)\Delta\boldsymbol{\lambda} - \Delta\boldsymbol{\theta}_G^T K_D\Delta\boldsymbol{\omega} \\
& + \alpha\gamma\Delta\hat{\boldsymbol{\theta}}_G^T R_1^T\Delta\hat{\boldsymbol{\omega}} + \Delta\boldsymbol{\theta}_G^T(\Lambda + \beta\mathcal{B}_r)\Delta\boldsymbol{\lambda} \\
& + \beta\gamma\Delta\hat{\boldsymbol{\theta}}_G^T R_3^T\Delta\hat{\boldsymbol{\lambda}} + \beta\Delta\boldsymbol{\lambda}^T(K_D + LT)\Delta\boldsymbol{\omega}. \qquad (43)
\end{aligned}$$

Define a state transformation matrix $T_L = [\boldsymbol{\nu}_{L1}, N_L]^T$, where $N_L = [\boldsymbol{\nu}_{L2}, \cdots, \boldsymbol{\nu}_{Lq}]$ and $\boldsymbol{\nu}_{Li}$ is the left eigenvector corresponding to eigenvalue $\lambda_i(L)$ for all $i \in \mathcal{S}_{\text{gen}}$. Specifically, $\boldsymbol{\nu}_{L1} = \mathbf{1}_q$ corresponds to $\lambda_1(L) = 0$ since L is a symmetrical and irreducible Laplacian matrix. Note also that the rest eigenvalues $\lambda_2(L), \cdots, \lambda_q(L)$ of L are positive [17]. The state transformation leads to $T_L\Delta\boldsymbol{\lambda} = [\delta\lambda_1, \delta\boldsymbol{\lambda}^T]^T \Rightarrow \Delta\boldsymbol{\lambda} = \boldsymbol{\nu}_{L1}\delta\lambda_1 + N_L\delta\boldsymbol{\lambda}$, where $\delta\lambda_1$ and $\delta\boldsymbol{\lambda} \in \mathbb{R}^{q-1}$ are the transformed states.

$$\begin{aligned}
\dot{V} \leq & - \delta\boldsymbol{\theta}_G^T B_r'\delta\boldsymbol{\theta}_G + \gamma\delta\hat{\boldsymbol{\theta}}_G^T(\hat{N}_B^T R_2\hat{N}_B)\delta\hat{\boldsymbol{\theta}}_G - \Delta\boldsymbol{\omega}^T M_1\Delta\boldsymbol{\omega} \\
& - (\delta\lambda_1\boldsymbol{\nu}_{L1}^T + \delta\boldsymbol{\lambda}^T N_L^T)(2\alpha L + \beta\Lambda)(\boldsymbol{\nu}_{L1}\delta\lambda_1 + N_L\delta\boldsymbol{\lambda}) \\
& - \delta\boldsymbol{\theta}_G^T N_B^T K_D\Delta\boldsymbol{\omega} + \alpha\gamma\delta\hat{\boldsymbol{\theta}}_G^T\hat{N}_B^T R_1^T\Delta\hat{\boldsymbol{\omega}} \\
& + \delta\boldsymbol{\theta}_G^T N_B^T(\Lambda + \beta\mathcal{B}_r)(\boldsymbol{\nu}_{L1}\delta\lambda_1 + N_L\delta\boldsymbol{\lambda}) \\
& + \beta\gamma\delta\hat{\boldsymbol{\theta}}_G^T\hat{N}_B^T R_3^T(\boldsymbol{\nu}_{L1}|\delta\lambda_1| + \hat{N}_L\delta\boldsymbol{\lambda}) \\
& + \beta(\delta\lambda_1\boldsymbol{\nu}_{L1}^T + \delta\boldsymbol{\lambda}^T N_L^T)(K_D + LT)\Delta\boldsymbol{\omega} \\
\leq & - \lambda_{\min}(M_2)\delta\hat{\boldsymbol{\theta}}_G^T\delta\hat{\boldsymbol{\theta}}_G - \lambda_{\min}(M_1)\Delta\hat{\boldsymbol{\omega}}^T\Delta\hat{\boldsymbol{\omega}} \\
& - \alpha\lambda_{\min}(L')\delta\hat{\boldsymbol{\lambda}}^T\delta\hat{\boldsymbol{\lambda}} - \beta\sum_{i=1}^{q}\frac{1}{2a_i}\delta\lambda_1^2 \\
& + \delta\hat{\boldsymbol{\theta}}_G^T(\widehat{N_B^T K_D} + \alpha\gamma\hat{N}_B^T R_1^T)\Delta\hat{\boldsymbol{\omega}} \\
& + \delta\hat{\boldsymbol{\theta}}_G^T(\widehat{N_B^T\Lambda\boldsymbol{\nu}_{L1}} + \beta\gamma\hat{N}_B^T R_3\boldsymbol{\nu}_{L1})|\delta\lambda_1| \\
& + \delta\hat{\boldsymbol{\theta}}_G^T\left(N_B^T(\widehat{\Lambda + \beta\mathcal{B}_r})N_L + \beta\gamma\hat{N}_B^T R_3^T\hat{N}_L\right)\delta\hat{\boldsymbol{\lambda}} \\
& + \beta\delta\lambda_1\boldsymbol{\nu}_{L1}^T(K_D + LT)\Delta\boldsymbol{\omega} + \beta\delta\boldsymbol{\lambda}^T N_L^T(K_D + LT)\Delta\boldsymbol{\omega} \\
& + 2\beta\delta\hat{\boldsymbol{\lambda}}^T\widehat{N_L^T\Lambda\boldsymbol{\nu}_{L1}}|\delta\lambda_1|. \qquad (44)
\end{aligned}$$

By applying state transformation to $\Delta\boldsymbol{\theta}_G$ and $\Delta\boldsymbol{\lambda}$, eq. (43) leads to (44) above, where $\lambda_{\min}(\cdot)$ means the minimum eigenvalue of the matrix, and

$$\begin{aligned}
M_2 &= \lambda_{\min}(\mathcal{B}_r')I_{q-1} - \gamma\hat{N}_B^T R_2\hat{N}_B, \\
L' &= N_L^T L N_L = \text{diag}\{[\lambda_2(L), \cdots, \lambda_q(L)]\}.
\end{aligned}$$

The second inequality in (44) follows from the inequality $\boldsymbol{x}^T A\boldsymbol{x} \geq \lambda_{\min}(A)\|\boldsymbol{x}\|^2$. It can be inferred that its first line is negative definite since $\lambda_{\min}(\mathcal{B}_r') > 0$, thus $\lambda_{\min}(M_2) > 0$ when γ is small enough. Also, $\lambda_{\min}(M_1) > 0$ when $\alpha \gg \beta > 0$, and $\lambda_{\min}(L') = \min\{\lambda_2(L), \cdots, \lambda_q(L)\} > 0$. The last three lines of the second inequality is indefinite, but these indefinite terms can be bounded by the negative definite terms by invoking inequality $\|\boldsymbol{a}\|^2 + \|\boldsymbol{b}\|^2 \geq 2\boldsymbol{a}^T\boldsymbol{b}$ when $\alpha \gg \beta > 0$ and γ is small enough, thus $\dot{V}$ is negative definite.

It can be concluded that the error system (39) is Lyapunov stable. In the steady state, the optimal solution of problem (10) is achieved, which corresponds to a sub-optimal solution of the original optimization problem (8). This concludes the proof of Theorem 1.

$$\begin{aligned}
-2\alpha\Delta\boldsymbol{\omega}^T\Lambda\Delta\boldsymbol{F} &= -\alpha\gamma\sum_{i=1}^{q}\left\{\frac{1}{a_i}\Delta\omega_i\sum_{(j,k)\in\mathcal{S}_{\text{crit}}} d_i^{jk}\{[F_{j,k} - \bar{F}_{j,k}]_+ - [F_{jk}^* - \bar{F}_{j,k}]_+\}\right\} \\
&\leq \alpha\gamma\sum_{i=1}^{q}\left\{\frac{1}{a_i}|\Delta\omega_i|\sum_{(j,k)\in\mathcal{S}_{\text{crit}}}|d_i^{jk}||\Delta F_{j,k}|\right\} \leq 2\alpha\gamma\Delta\hat{\boldsymbol{\omega}}^T\Lambda\hat{\boldsymbol{d}}_{jk}\hat{\boldsymbol{\phi}}_{jk}^T\Delta\hat{\boldsymbol{\theta}}_G \triangleq \alpha\gamma\Delta\hat{\boldsymbol{\omega}}^T R_1\Delta\hat{\boldsymbol{\theta}}_G
\end{aligned} \qquad (42)$$

APPENDIX B
KEY PARAMETERS OF THE CASE STUDIES

TABLE V
PARAMETERS OF THE DGS IN THE IEEE 34-BUS MICRO-GRID

GU No.	Bus No.	Cost Parameters			$P_i^{\min}$	$P_i^{\max}$	k_{Di}
		a_i	b_i	c_i	(MW)	(MW)	(MW/Hz)
1	800	1.00	1.0	0.4	0	0.7	0.2
2	808	0.95	1.1	0.4	0	0.7	0.2
3	822	0.85	1.3	0.4	0	0.7	0.2
4	826	0.90	1.2	0.4	0	0.7	0.2
5	832	0.65	1.7	0.4	0	0.7	0.2
6	838	0.70	1.6	0.4	0	0.8	0.2
7	840	0.75	1.5	0.4	0	0.8	0.2
8	848	0.80	1.4	0.4	0	0.8	0.2
9	856	0.60	1.8	0.4	0	0.8	0.2
10	806	1.00	1.0	0.4	0	0.8	0.2

TABLE VI
PARAMETERS OF THE GUS IN THE IEEE 118-BUS SYSTEM

GU No.	Bus No.	Cost Parameters			$P_i^{\min}$	$P_i^{\max}$	k_{Di}
		a_i	b_i	c_i	(MW)	(MW)	(MW/Hz)
1	10	0.0889	20	100	55	550	20
2	12	0.2333	20	100	18	185	8
3	25	0.135	20	100	32	320	16
4	26	0.0954	20	100	41	414	20
5	31	0.711	20	100	10	107	5
6	46	0.5263	20	100	12	119	6
7	49	0.131	20	100	30	304	15
8	54	0.311	20	100	15	148	7
9	59	0.1613	20	100	25	255	12
10	61	0.1563	20	100	26	260	10
11	65	0.1024	20	100	49	490	20
12	66	0.1021	20	100	49	490	15
13	69	0.0772	20	100	80	805	35
14	80	0.0836	20	100	55	577	25
15	87	1.251	20	100	10	104	5
16	89	0.099	20	100	70	707	30
17	100	0.141	20	100	35	352	15
18	103	0.3705	20	100	14	140	7
19	111	0.4051	20	100	13	136	7

TABLE VII
PARAMETERS OF THE CRITICAL LINES IN THE IEEE 118-BUS SYSTEM

Critical Line No.	From Bus No.	To Bus No.	Thermal Limit (MW)	$\bar{F}_{i,j}$ (MW)
1	25	23	215	214
2	26	30	240	239
3	65	38	205	204
4	65	68	220	219

REFERENCES

[1] P. Kundur, *Power System Stability and Control*. 1st ed., New York, NY, USA: McGraw-Hill, 2006.

[2] A. Bidram and A. Davoudi, "Hierarchical structure of microgrids control system," *IEEE Trans. Smart Grid*, vol. 3, no. 4, pp. 1963–1976, Dec. 2012.

[3] F. Dörfler, J. Simpson-Porco, and F. Bullo, "Plug-and-play control and optimization in microgrids," in *Proc. IEEE Conf. Decision Control*, Dec. 15–17, 2014, pp. 211–216.

[4] D. Gan, D. Feng, and J. Xie, *Electricity Markets and Power System Economics*, 1st ed. Boca Raton, FL, USA: CRC Press, 2013.

[5] N. Amjady, F. Keynia, and H. Zareipour, "Short-term load forecast of microgrids by a new bilevel prediction strategy," *IEEE Trans Smart Grid*, vol. 1, no. 3, pp. 286–294, Dec. 2010.

[6] M. Ilić, "From hierarchical to open access electric power systems," *Proc. IEEE*, vol. 95, no. 5, pp. 1060–1084, May 2007.

[7] C. Gungor, D. Sahin, T. Kocak, S. Ergut, *et al.*, "A survey on smart grid potential applications and communication requirements," *IEEE Trans. Ind. Informat.*, vol. 9, no. 1, pp. 28–42, Feb. 2013.

[8] X. Fang, S. Misra, G. Xue, and D. Yang, "Managing smart grid information in the cloud: Opportunities, model, and applications," *IEEE Netw.*, vol. 26, no. 4, pp. 32–38, Jul./Aug. 2012.

[9] B. Millar, D. Jiang, and M. E. Haque, "Constrained coordinated distributed control of smart grid with asynchronous information exchange," *J. Mod. Power Syst. Clean Energy*, vol. 3, no. 4, pp. 512–525, Dec. 2015.

[10] Z. Zhang and M.-Y. Chow, "Convergence analysis of the incremental cost consensus algorithm under different communication network topologies in a smart grid," *IEEE Trans. Power Syst.*, vol. 27, no. 4, pp. 1761–1768, Nov. 2012.

[11] S. Yang, S. Tan, and J.-X. Xu, "Consensus based approach for economic dispatch problem in a smart grid," *IEEE Trans. Power Syst.*, vol. 28, no. 4, pp. 4416–4426, Nov. 2013.

[12] W. Zhang, W. Liu, X. Wang, L. Liu, and F. Ferrese, "Online optimal generation control based on constrained distributed gradient algorithm," *IEEE Trans. Power Syst.*, vol. 30, no. 1, pp. 35–45, Jan. 2015.

[13] H. Xin, L. Zhang, Z. Wang, D. Gan, *et al.*, "Control of island AC microgrids using a fully distributed approach," *IEEE Trans. Smart Grid*, vol. 6, no. 2, pp. 943–945, Mar. 2015.

[14] Z. Miao and L. Fan, "Achieving economic operation and secondary frequency regulation simultaneously through feedback control," *IEEE Trans. Power Syst.*, vol. 31, no. 4, pp. 3324–3325, Jul. 2015.

[15] J. Mohammadi, G. Hug, and S. Kar, "Fully distributed DC-OPF approach for power flow control," in *Proc. IEEE Power Eng. Soc. General Meeting*, 2015, pp. 1–5.

[16] A. Wood and B. Wollenberg, *Power Generation, Operation, and Control*, 3rd ed. Hoboken, NJ, USA: Wiley, 2013.

[17] Z. Qu, *Cooperative Control of Dynamical Systems*, 1st ed. London, U.K.: Springer-Verlag, 2009.

[18] D. Pudjianto, C. Ramsay, and G. Strbac, "Virtual power plant and system integration of distributed energy resources," *IET Renew. Power Gener.*, vol. 1, no. 1, pp. 10–16, Mar. 2007.

[19] H. Xin, D. Gan, N. Li, H. Li, and C. Dai, "Virtual power plant-based distributed control strategy for multiple distributed generators," *IET Control Theory Appl.*, vol. 7, no. 1, pp. 90–98, Jan. 2013.

[20] Y. Li and F. Nejabatkhah, "Overview of control, integration and energy management of microgrids," *J. Mod. Power Syst. Clean Energy*, vol. 2, no. 3, pp. 212–222, Sep. 2014.

[21] D. Wu, F. Tang, T. Dragicevic, J. C. Vasquez, and J. M. Guerrero, "Autonomous active power control for islanded ac microgrids with photovoltaic generation and energy storage system," *IEEE Trans. Energy Convers.*, vol. 29, no. 4, pp. 882–892, Dec. 2014.

[22] L.-R. Chang-Chien and Y.-C. Yin, "Strategies for operating wind power in a similar manner of conventional power plant," *IEEE Trans. Energy Convers.*, vol. 24, no. 4, pp. 926–934, Dec. 2009.

[23] H. Xin, Y. Liu, Z. Wang, D. Gan, and T. Yang, "A new frequency regulation strategy for photovoltaic systems without energy storage," *IEEE Trans. Sustain. Energy*, vol. 4, no. 4, pp. 985–993, Oct. 2013.

[24] M. Wooldridge, *An Introduction to Multiagent Systems*, 2nd ed. West Sussex, U.K.: Wiley, 2009.

[25] F. Eddy, H. B. Gooi, and S. X. Chen, "Multi-agent system for distributed management of microgrids," *IEEE Trans. Power Syst.*, vol. 30, no. 1, pp. 24–34, Jan. 2015.

[26] S. D'Arco and J. A. Suul, "Equivalence of virtual synchronous machines and frequency-droops for converter-based microgrids," *IEEE Trans. Smart Grid*, vol. 5, no. 1, pp. 394–395, Jan. 2014.

[27] A. Maknouninejad and Z. Qu, "Realizing unified microgrid voltage profile and loss minimization: A cooperative distributed optimization and control approach," *IEEE Trans. Smart Grid*, vol. 5, no. 4, pp. 1621–1630, Jul. 2014.

[28] S. Bolognani, R. Carli, G. Cavraro, and S. Zampieri, "Distributed reactive power feedback control for voltage regulation and loss minimization," *IEEE Trans. Autom. Control*, vol. 60, no. 4, pp. 966–981, Apr. 2015.

[29] G. Binetti, A. Davoudi, F. L. Lewis, D. Naso, and B. Turchiano, "Distributed consensus-based economic dispatch with transmission losses," *IEEE Trans. Power Syst.*, vol. 29, no. 4, pp. 1711–1720, Jul. 2014.
[30] S. Boyd and L. Vandenberghe, *Convex Optimization*, 1st ed. Cambridge, U.K.: Cambridge Univ. Press, 2004.
[31] K. Purchala, L. Meeus, D. Van Dommelen, and R. Belmans, "Usefulness of dc power flow for active power flow analysis," in *Proc. IEEE Power Eng. Soc. General Meeting*, Jun. 12–15, 2005, pp. 454–459.
[32] R. D. Zimmerman, C. E. Murillo-Sánchez, and R. J. Thomas, "Matpower: Steady-state operations, planning, and analysis tools for power systems research and education," *IEEE Trans. Power Syst.*, vol. 26, no. 1, pp. 12–19, Feb. 2011.

Yun Liu (S'14–M'16) received the B.Eng. (Hons.) degree and the Ph.D. degree from the College of Electrical Engineering, Zhejiang University, Hangzhou, China, in June 2011 and June 2016, respectively. He is currently a Research Fellow in the Energy Research Institute, Nanyang Technological University, Singapore. He was a visiting student in the Department of Electrical Engineering and Computer Science, University of Central Florida, Orlando, FL, USA, from August 2014 to September 2015. His research interests include power system stability analysis and distributed control of renewable energy.

Zhihua Qu (M'90–SM'93–F'09) received the Ph.D. degree in electrical engineering from Georgia Institute of Technology, Atlanta, GA, USA, in June 1990. Since then, he has been with the University of Central Florida (UCF), Orlando, FL, USA, currently as a Professor and the Chair of ECE. He is the SAIC Endowed Professor of UCF. His areas of expertise are nonlinear systems and control, energy and power systems, and autonomous vehicles and robotics. In energy systems, his research covers such subjects as low-speed power generation, dynamic stability of distributed power systems, anti-islanding control and protection, distributed generation and load sharing control, distributed VAR compensation, and distributed optimization and cooperative control.

Huanhai Xin (M'14) received the Ph.D. degree from the College of Electrical Engineering, Zhejiang University, Hangzhou, China, in June 2007. He was a Postdoctor in the Electrical Engineering and Computer Science Department, University of Central Florida, Orlando, FL, USA, from June 2009 to July 2010. He is currently a Professor in the Department of Electrical Engineering, Zhejiang University. His research interests include distributed control in active distribution grid and microgird, AC/DC power system transient stability analysis and control, and grid integration of large-scale renewable energy to weak grid.

Deqiang Gan (M'96–SM'01) received the Ph.D. degree from Xi'an Jiaotong University, Xi'an, China, in 1994. He has been a faculty member with Zhejiang University, Hangzhou, China, since 2002. His employment experience includes ISO New England, Inc., Ibaraki University, University of Central Florida, and Cornell University. His research interests include power system stability and market operations. He is currently an Editor of *International Transactions on Electrical Energy Systems*.